JACS
JOURNAL OF THE AMERICAN CHEMICAL SOCIETY
Article
Cite This: J. Am. Chem. Soc. 2020, 142, 857−866
pubs.acs.org/JACS

Gyroid and Other Ordered Morphologies in Single-Ion Conducting Polymers and Their Impact on Ion Conductivity

Lu Yan,[†] Christina Rank,[§] Stefan Mecking,[§] and Karen I. Winey*[,†,∥]

[†]Department of Chemical and Biomolecular Engineering, The University of Pennsylvania, Philadelphia, Pennsylvania 19104, United States

[§]Department of Chemistry, University of Konstanz, Universitätsstraße 10, 78457 Konstanz, Germany

[∥]Department of Materials Science and Engineering, The University of Pennsylvania, Philadelphia, Pennsylvania 19104, United States

Supporting Information

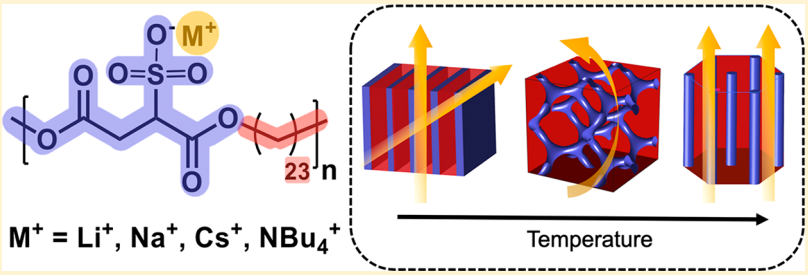

ABSTRACT: Controlling the self-assembled nanoscale ionic aggregates in single-ion conducting polymers is a crucial step toward exceptional transport properties. We report a series of precisely segmented polyethylene-like materials containing sulfonate groups (PES23) with Li^+, Na^+, Cs^+, or NBu_4^+ counterions synthesized from step-growth polymerization. At room temperature, all polymers are semicrystalline with well-defined nanoscale ionic layers separated by 35−38 Å, depending on the cation. *In situ* X-ray scattering measurements reveal that the layered ionic aggregates in PES23Li, PES23Na, and PES23Cs transform, upon melting the PE blocks, into the $Ia\bar{3}d$ gyroid morphology. The gyroidal ionic aggregates in PES23Li and PES23Na further evolve into hexagonal symmetry as the temperature increases. These order-to-order transitions in ionic aggregate morphologies were also confirmed by oscillatory shear rheology. The ion transport behavior of these PES23 polymers is strongly dependent on the ionic aggregate morphologies. Specifically, the 3D interconnected gyroid morphology of PES23Li exhibits higher ionic conductivity than the isotropic layered or hexagonal morphologies. This innovative and versatile molecular design of single-ion conducting polymers leads to unprecedented percolated gyroidal ionic aggregate morphologies that provide a continuous pathway for improved ion transport.

INTRODUCTION

The nanoscale morphologies within materials often determine their macroscopic properties. Thus, methods for controlling nanoscale morphologies, by processing or materials design, are highly desirable for developing advanced materials for the most challenging applications, e.g., superior polymer electrolytes for various energy applications.[1−6] It is well-established that linear block copolymers, including diblocks, triblocks, and multiblocks, as well as nonlinear cyclic and branched block copolymers, microphase separate into various nanostructures as a result of the hierarchical molecular conformations.[7−10] Recently, a rich assortment of nanostructured block copolymers have been designed and tested to improve transport properties with potential applications in lithium-ion batteries, fuel cells, and superconductors.[11−16] While the layered morphology (LAM), and hexagonally packed cylinders (HEX) exhibit only 2D or 1D connectivity, respectively, the bicontinuous gyroid morphology (GYR) attracts special interests. The three-dimensional interconnected networks in GYR provide a structural advantage that reduces the energy barriers for ion diffusion across grain boundaries and promotes more efficient transport.[17−22] These cubic gyroid morphologies were recently reported for various ion transport applications in a variety of experimental[2,12,18−20,22−24] and computational[25−29] studies of diblock copolymers[22,24] and small molecule liquid crystals.[12,18,19,30] Wiesner and co-workers observed that the ionic conductivity in a cubic double gyroid structure is close to an order of magnitude higher than the hexagonal cylinder morphology in poly(ethylene oxide) (PEO)-based dendrons.[31] Similarly, Kato et al. reported that the gyroid phase exhibits nearly an order of magnitude higher ionic conductivity than the hexagonal columnar and disordered phases in ammonium salts-based liquid crystals.[23,32] Park et al. demonstrated a 2-fold improved normalized ionic conductivity in the gyroid morphology compared to the disordered phase in ionic liquid doped sulfonated polystyrene-*co*-polymethylbutylene diblock copolymers.[33]

Received: September 7, 2019
Published: December 6, 2019

DOI: 10.1021/jacs.9b09701
J. Am. Chem. Soc. 2020, 142, 857−866

Scheme 1. Molecular Structure of PES23M Polymers, where M^+ is Li^+, Na^+, Cs^+, or NBu_4^+

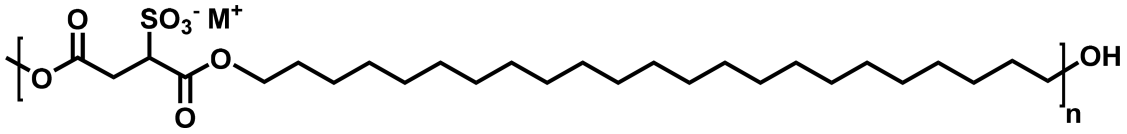

Table 1. Summary of the Polyethylene Sulfonates Synthesized and Materials Information

polymer	DP_n[a]	M_n (kg/mol)	f_{polar}[b]	cation size (Å)	T_{endo} (°C)[c]	T_{exo} (°C)	type of morphology transition[f]
PES23Li	22.5	11.8	0.27	0.76[47]	123.1[d]	90.1	LAY-GYR
					175.9	168.1	GYR-HEX
PES23Na	21.0	11.3	0.27	1.02	126.6[e]	–	LAY-GYR
					193.7	153.4	GYR-HEX
PES23Cs	21.5	14.0	0.29	1.67	139.3	120.5	LAY-GYR
$PES23NBu_4$	21.5	16.7	0.52	4.94[48]	31.9	29.6	LAY-DIS
PE23	26.0	14.8	–	–	90.8	81.0	LAY-DIS

[a]The degree of polymerization was determined from ^1H NMR (Figures S1–S6). [b]The volume fraction of the sulfosuccinate blocks. [c]The thermal transition temperatures according to DSC typically measured at 10 °C/min. [d]PES23Li was measured at a ramp rate of 1 °C/min. [e]The melting temperature of PES23Na is measured 3 days after the first cycle due to the slow crystallization. [f]LAY, GYR, HEX, and DIS represents layered, gyroid, hexagonal, and disordered ionic aggregate morphologies, respectively.

Most of the aforementioned gyroid morphologies require the addition of lithium salts or ionic liquids to both produce the gyroid structure and provide mobile ions to conduct. In contrast, single-ion conductors are polymers with covalently bonded anions to the polymer backbone with associated counterions, commonly termed ionomers. Under applied electric fields, the tethered anions on ionomers are comparatively immobile in the melt state relative to the mobile cations because ion motion is commonly coupled with the slow polymer segmental relaxation.[34−36] Consequently, single-ion conducting polymers can circumvent the shortcomings of salt-based systems, in which anions migrate to and polarize the electrodes. Nonetheless, single-ion conductors continue to exhibit discouragingly low ionic conductivities across a wide range of materials systems for two primary reasons: ionomers microphase separate to form discrete, nominally ionic aggregates and cations are tightly associated with the anion on the polymer. Transporting cations between discrete ionic aggregates requires the discrete aggregates to merge, exchange counterions, and separate again, which relies on extensive polymer backbone rearrangement. In contrast, this study focuses on designing new single-ion conducting polymers to produce highly interconnected ionic nanoscale domains to facilitate cation mobility through percolated and redundant pathways.

Recent advances in polymer synthesis render new opportunities to control ion aggregation through modifying the polymer architecture. Winey and co-workers reported the morphologies of a series precise acid- and ion-containing polyethylenes synthesized from acyclic diene metathesis.[37−42] The acid or ionic groups in those precise polyethylenes are evenly spaced along a linear backbone and thus the polymers microphase separate into well-ordered ionic aggregate morphologies compared to the randomly functionalized ionomers. When the polyethylene (PE) spacer is long enough to crystallize, these precise polyethylenes can form unique hairpin chain-folded chain conformations with acidic or ionic layers stacked within the crystallites.[42−44] This acid layered morphology exhibits efficient proton conductivity at 40 °C when hydrated (>60% relative humidity).[45] The metal cation transport in similar ionic layers under the anhydrous condition was further studied in a series of monodisperse and telechelic polyethylenes, and ion transport is decoupled from the polymer segmental motion in those ionic layers, although still low due to a combination of limited cation dissociation and discontinuities between the layered aggregates at grain boundaries.[46] A greater connectivity of the ionic aggregates should improve conductivity. However, to our knowledge, the mostly highly interconnected structures in microphase separated polymers, such as the gyroid structure, has not been reported or exploited in single-ion conductors of any type.

Here, we report, for the first time, the bicontinuous gyroid structure in single-ion conducting ionomers. This is demonstrated for readily accessible novel ion-containing polyethylenes with periodically sequenced sulfonate groups. These periodic polyethylenes are comprised of short polar segments and long nonpolar PE segments. The gyroid morphology exhibits higher shear modulus and superior ion transport properties compared to the layered and hexagonal morphologies. This work both demonstrates the ability to control the nanostructured morphology by manipulating the polymer architecture in single-ion conductors and expands the portfolio of available ordered nanostructures to include the bicontinuous gyroid structure, which has promising implications for transport in solid polymer electrolytes.

RESULTS AND DISCUSSION

Chemical Structure and Thermal Properties. The periodic PE sulfonates studied herein were synthesized by step-growth polymerization chemistry. In a classical melt polyesterification, tetra-*n*-butylammonium dimethylsulfosuccinate and 1,23-tricosanediol were polymerized to the tetrabutylammonium-substituted ionomer ($PES23NBu_4$). Subsequent ion exchange yielded the lithium, sodium, and cesium substituted ionomers (PES23Li, PES23Na, and PES23Cs), respectively. Detailed experimental procedures and NMR spectra are described in the Supporting Information. Scheme 1 displays the molecular structure of the polymers, in which the sulfosuccinate blocks are periodically separated by precisely 23 methylene units (PES23). A nonionic version of the

DOI: 10.1021/jacs.9b09701
J. Am. Chem. Soc. 2020, 142, 857−866

polymer (PE23) without the pendant sulfonate groups was also synthesized for comparison, see Supporting Information.

Table 1 summarizes the basic physical and thermal properties of PE23 and the PES23 polymers. The volume fractions of the polar sulfosuccinate blocks, which were calculated through the van der Waals volume using Chemicalize software, increase from 0.28 to 0.53 when the cation size increases from Li^+ to NBu_4^+. Driven by the crystallization tendency of the long PE block, all polymers are semicrystalline at room temperature and exhibit a melting temperature as evidenced by DSC. Due to the slow crystal growth rates in PES23Li, a 1 °C/min cooling rate was used to observe crystallization. PES23Na crystallizes even more slowly and exhibits a melting point after 3 days at room temperature (Figure S7). The melting temperatures (T_m) of PES23Li, PES23Na, and PES23Cs are 120−130 °C, while the T_m is significantly lower for $PES23NBu_4$ (32 °C). This indicates that the large ammonium cation significantly impedes the dense packing of the PE segments into crystallites. Interestingly, PES23Li and PES23Na show an additional thermal transition at 176 and 194 °C, respectively, that will be explored by *in situ* X-ray scattering.

The Bicontinuous Gyroid Morphology. Recently, we reported a similar series of copolymers with alternating high dielectric constant sulfosuccinate blocks and low dielectric constant PE blocks.[49] The ionic groups in those polymers self-assemble into stacks of ionic layers embedded in the PE crystallites and the ionic layers transform into hexagonal symmetry upon the melting of the PE blocks. Remarkably, new bicontinuous gyroid structures form in PES23Li, PES23Na, and PES23Cs at elevated temperatures. Figure 1 displays the

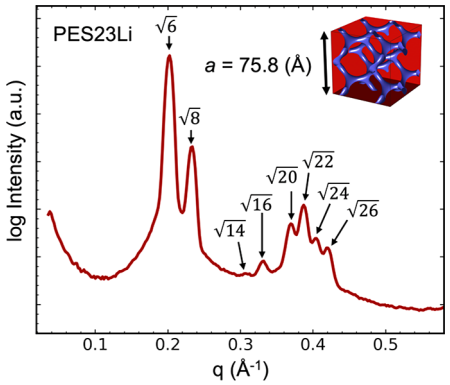

Figure 1. Small-angle X-ray scattering profile of PES23Li at 150 °C exhibits the $Ia\bar{3}d$ cubical gyroid phase. The ratios of the Bragg peaks are labeled.

small-angle X-ray scattering data of PES23Li at 150 °C. The Bragg peaks at $\sqrt{6}\,q^*$, $\sqrt{8}\,q^*$,$\sqrt{14}\,q^*$, $\sqrt{16}\,q^*$, $\sqrt{20}\,q^*$, $\sqrt{22}\,q^*$, $\sqrt{24}\,q^*$, and $\sqrt{26}\,q^*$ correspond to the (211), (220), (321), (400), (420), (332), (422), and (431) reflections of a $Ia\bar{3}d$ gyroid phase with a cubic unit cell dimension of a = 75.8 Å. Details regarding the peak positions are provided in Table S1. Note that the volume fraction of the polar block with the Li^+ cation is 0.27, which is similar to the volume fraction of amorphous diblock copolymers exhibit the bicontinuous gyroid morphology. This is the first report, to the best our knowledge, that a 3D interconnected ionic aggregate morphology has been identified experimentally in a neat ionomer, i.e., without added solvent or salt.

Morphological Transitions with Temperature. To further investigate the stability of the gyroid phase, *in situ* X-ray scattering was used to study the morphologies and thermal transitions. Figure 2 shows the small- and wide-angle X-ray scattering (SAXS and WAXS) data from the four PES23 polymers at selected temperatures during heating. All the morphological transformations within the measured temperature range are fully reversible (Figure S9).

At 30 °C, all four polymers exhibit a single crystalline peak at $q \approx 1.5$ $Å_{-1}$ indicating that the long PE blocks crystallize on a hexagonal lattice. The hexagonal crystal phase was observed in linear PEs at elevated temperatures with $q_{(100)}$ = 1.48 $Å^{-1}$ and a_{hex} = 4.88 Å[50,51] and was recently identified in a series of precise acid- and ion-containing polyethylenes.[43−45] Unit cell parameters of the hexagonal lattice are provided in Table S2. The pendant sulfonate groups are packed into stacks of layers as evidenced by the Bragg reflections in the small q-range with position ratios (q/q^*) of 1:2:3:4 and layer-to-layer distances (d_{layer}) of ∼35−38 Å (Table 2). The hexagonal packing of the backbones and a tight chain folding conformation have been elucidated previously in our studies on three precise ion- and acid-functionalized polyethylenes.[43−45] Thus, it is reasonable to infer that the PES23 polymers adopt a similar chain folding motif at the polar block to allow the ionic groups to form layers. This polymer conformation satisfies the attractive interactions between polar groups ($SO_3^-M^+$) while allowing the PE segments to crystallize. Further evidence for this morphology includes the d_{layer} values observed for the PES23 polymers, which are consistent with an all *trans* monomeric backbone (35.2 Å), the sulfonate/cation size, and varying degrees of chain tilt.

Upon heating above the first thermal transition temperature, the crystalline peak at $q \approx 1.5$ $Å_{-1}$ disappears, and a broad amorphous halo related to the average backbone-to-backbone spacing appears between 1.3 and 1.4 $Å^{-1}$, indicating the melting of the PE crystallites, Figure 2. Accompanying this PE melting, the ionic aggregates in PES23Li, PES23Na, and PES23Cs transforms from layered structures to bicontinuous gyroid morphologies exhibiting the $Ia\bar{3}d$ space group. The cubic gyroid structures of PES23Na and PES23Cs resemble the one formed in PES23Li (Figure 1), and the polar volume fractions are comparable (0.27−0.29), Table 1. In contrast, the layered ionic aggregates in $PES23NBu_4$ directly transform into disordered aggregates upon melting with an average inter-aggregate distance of 27.6 Å; this liquid-like order of ionic aggregate morphology is typical with most ionomer melts.[37,52] The absence of the gyroid in $PES23NBu_4$ is attributed to the larger polar volume fraction in $PES23NBu_4$, 0.52, being incompatible with the gyroid morphology. The gyroid structure in ionomers appears to require an amorphous polymer backbone ($T > T_m$), a well-defined polymer microstructure, and a polar volume fraction of ∼0.28.

Further increasing the temperature to 170−190 °C leads to another phase transition in PES23Li and PES23Na, which correlates with the transformation of gyroid ionic aggregates to hexagonal symmetry. The hexagonally packed ionic aggregates in PES23Li at 170 °C and PES23Na at 190 °C give rise to the Bragg reflections of q^*, $\sqrt{3}\,q^*$ and $\sqrt{4}\,q^*$, with $d_{100} = 2\pi/q^*$ = 26.2 and 27.0 Å, respectively. The gyroid phase in PES23Cs persists to 210 °C with no additional phase transitions. Both the well-defined chemistry and the strongly interacting ionic forces in the PES23 polymers are essential in forming ordered ionic aggregate morphologies.

DOI: 10.1021/jacs.9b09701
J. Am. Chem. Soc. 2020, 142, 857−866

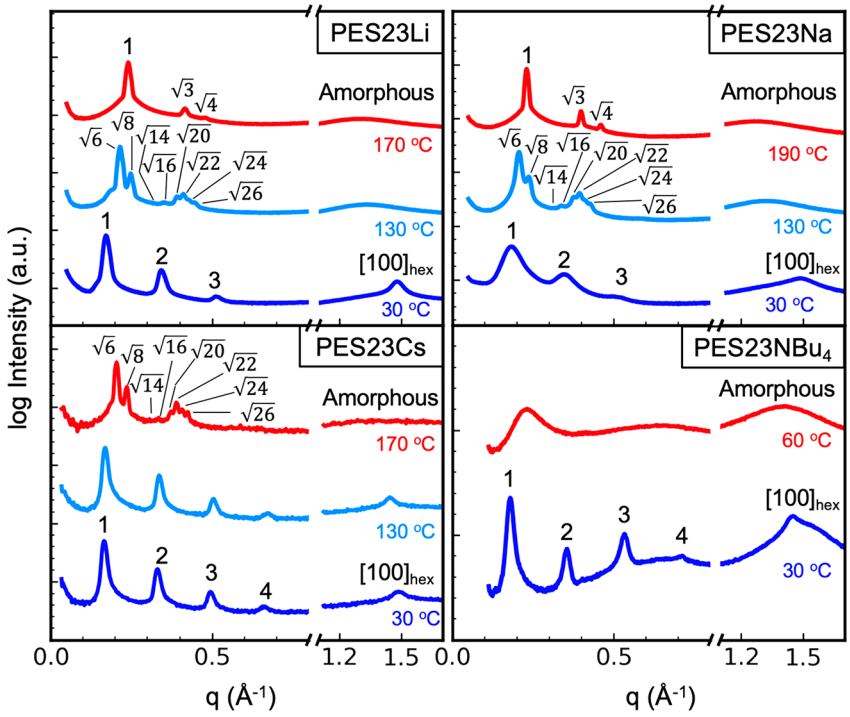

Figure 2. *In situ* X-ray scattering profiles of (a) PES23Li, (b) PES23Na, (c) PES23Cs, and (d) $PES23NBu_4$ at selected temperatures during the second heating. Data are shifted vertically for clarity. Ratios of the Bragg peaks are as labeled. $[100]_{hex}$ denotes that the PE blocks are packed on a hexagonal lattice leading to the [100] Bragg reflection. Complete *in situ* X-ray scattering data from heating and cooling cycles are available in Figure S9 and indicate full reversibility.

Table 2. Ionic Aggregate Morphologies of PES23 Polymers

polymer	temp (°C)	morphology type	morphological parameter (Å)[a]
PES23Li	30	layered	36.7
	130	gyroid	69.9
	170	hexagonal	30.2
PES23Na	30	layered	34.9
	130	gyroid	72.6
	190	hexagonal	31.1
PES23Cs	30	layered	38.1
	170	gyroid	75.4
$PES23NBu_4$	30	layered	35.5
	60	disordered	27.5

[a]Morphological parameter: $d_{layer} = hd_h$; $a_{cub} = d_{hkl}\,(h^2 + k^2 + l^2)^{1/2}$; $d_{disordered} = d^* = 2\pi/q^*$.

Phase Diagram of PES23 Polymers. Figure 3 summarizes the morphologies of PES23 ionomers as a function of temperature as determined by *in situ* X-ray scattering and includes both the PE backbone structure (symbols) and the morphology of the ionic aggregates (shaded colors). The dash lines in the phase diagram denote the phase boundaries extracted from X-ray scattering, and there are temperatures where two morphologies coexistence.

The ionic aggregates in PES23Li and PES23Na undergo two order-to-order transitions (OOTs) upon heating: (1) the layered ionic aggregates transform to the gyroid phase with a small coexistence region at 100−120 °C; (2) the gyroid morphologies transition to hexagonal symmetries at higher temperatures. In PES23Na, the gyroid to hexagonal OOT

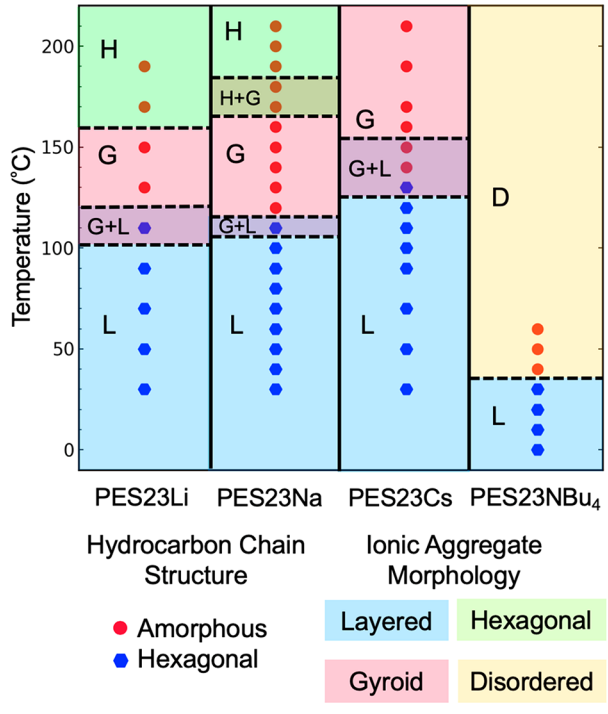

Figure 3. Morphology diagram of PES23 ionomers during the second heating in X-ray scattering. Blue hexagons and red circles represent PE backbone structures. L, G, H, and D letters denote layered, gyroid, hexagonal, and disordered ionic aggregate morphologies.

presents a coexistence region. PES23Cs only exhibits one OOT, i.e., from layers to gyroid, with a coexistence region at 130−160 °C. The coexistence regions (G + L and H + G) associated with these OOTs are attributed to the slow kinetics

DOI: 10.1021/jacs.9b09701
J. Am. Chem. Soc. 2020, 142, 857−866

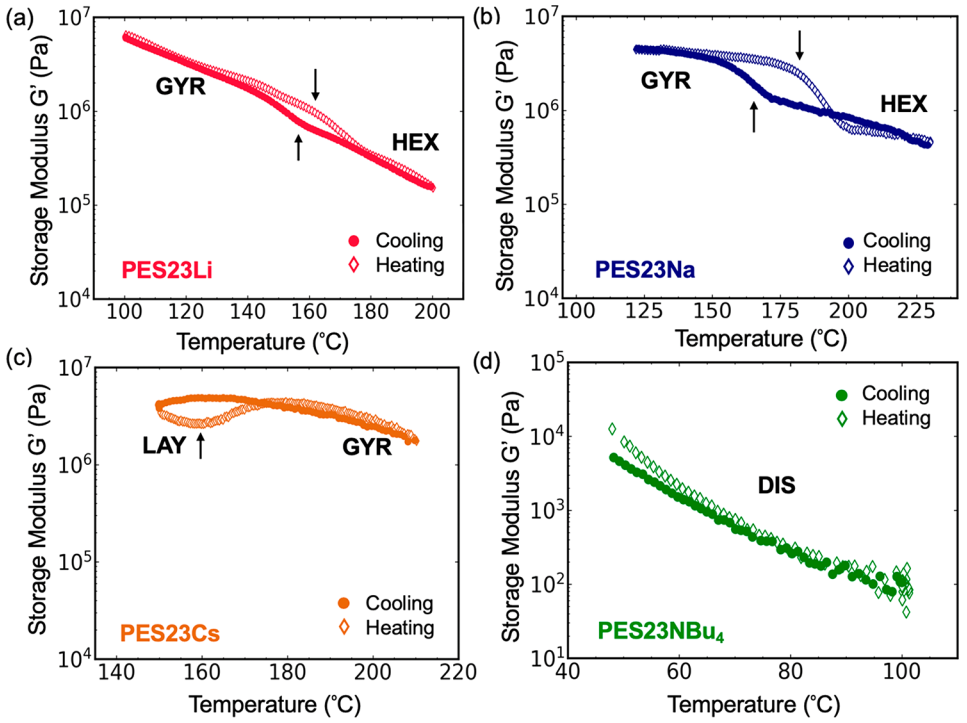

Figure 4. Melt-state storage modulus of PES23 ionomers as a function of temperature. Data is shown from the first cooling (filled symbols) and the second heating (open symbols) at a rate of 1 °C/min and a fixed oscillatory shear frequency of 1 rad/s. The black arrows indicate the onset of OOT during the cooling or heating. Note the different G' scale in (d).

of these transformations and will be evident in the rheological and conductivity measurements below. In PES23Cs, the gyroid morphology persists up to 210 °C, the highest experimental temperature employed.

Increasing the cation size to NBu_4^+ leads to simultaneous melting of the PE crystals and an order−disorder transition from layered to disordered ionic aggregates; $PES23NBu_4$ does not exhibit OOTs. The counterion size impacts both the volume fraction of the polar blocks in the ionomers and the strength of the electrostatic cohesion. Since the ionic radius of NBu_4^+ is 2−5 times larger than that Li^+, Na^+, and Cs^+, both the large f_{polar} (0.52) and the weakened electrostatic interaction in $PES23NBu_4$ impede the formation of the bicontinuous gyroid morphology. The gyroid structure in the minority phase of diblock copolymers is typically found at a volume fraction of 0.2−0.4.[8,28,53] The f_{polar} (0.27−0.29) here in PES23Li, PES23Na, and PES23Cs is consistent with conventional χN vs f phase diagram in amorphous diblock copolymers. Note that these PES23 polymer are structurally different from block copolymers, a direct comparison with block copolymer phase behavior would be difficult at this early stage. A gyroid structure with NBu_4^+ ions might be possible by employing a shorter alkyl block to reach an appropriate volume fraction.

Order-to-Order Transition (OOT). Linear viscoelastic properties are sensitive to microphase separated morphologies in diblock copolymers and have previously been used to detect OOTs in amorphous diblock copolymers. Figure 4 shows the storage modulus (G') as a function of temperature ($T > T_m$) upon the first cooling and second heating. The loss modulus (G'') data are provided in Figure S10.

When decreasing temperature from 200 °C, the storage modulus of PES23Li smoothly increases, consistent with the slowing of the segmental mobility. Notably, there is a slope change in G' at ∼160 °C that correlates to the hexagonal to gyroid OOT. This slope change in G' is also observable during the second heating at a slightly higher temperature, which is due to the hysteresis in the transformation from the cubic gyroid to hexagonal morphology. PES23Na exhibits a more pronounced drop in G' from 5×10^7 to 5×10^6 Pa when the gyroid phase transforms into hexagonal morphology upon heating (Figure 4b). Unlike PES23Li, the storage modulus of PES23Na in the gyroid structure depends only weakly on temperature, suggesting that the PES23Na gyroid phase is better developed and more mechanically robust. Figure 4 and 4b provide strong evidence of gyroid-hexagonal OOTs in PES23Li and PES23Na that is consistent with the thermal transitions observed in DSC and X-ray scattering.

The layered to gyroid OOTs in PES23Li and PES23Na occur below ∼125 °C and were not accessible by rheology. For PES23Cs, a change in the slope G' at ∼150 °C during cooling might indicate a gradual transition from gyroid to layered aggregates. The coexistence of gyroid and layered structure ∼150 °C is evidenced by SAXS data (Figure 3, Figure S9). This transition is more noticeable in the heating cycle where the transition from layered to gyroid aggregates corresponds to an increase in G'.

Finally, rheology confirms that ionic aggregates in $PES23NBu_4$ are disordered in that G' is smaller than G'' within the measured temperature window consistent with liquid-like behavior. Since $PES23NBu_4$ only exhibits a single phase above the melting point, no abrupt change is observed in G' during the temperature ramp (Figure 4d). The gradual modulus decrease during the heating is consistent with higher segmental mobility, as observed in the PES23Li.

Anhydrous Ionic Conductivities of PES23 Polymers. Figure 5a displays the temperature-dependent DC ionic conductivities of the PES23 ionomers during cooling; the non-ionic PE23 polymer is included for reference. PE23Li and

DOI: 10.1021/jacs.9b09701
J. Am. Chem. Soc. 2020, 142, 857−866

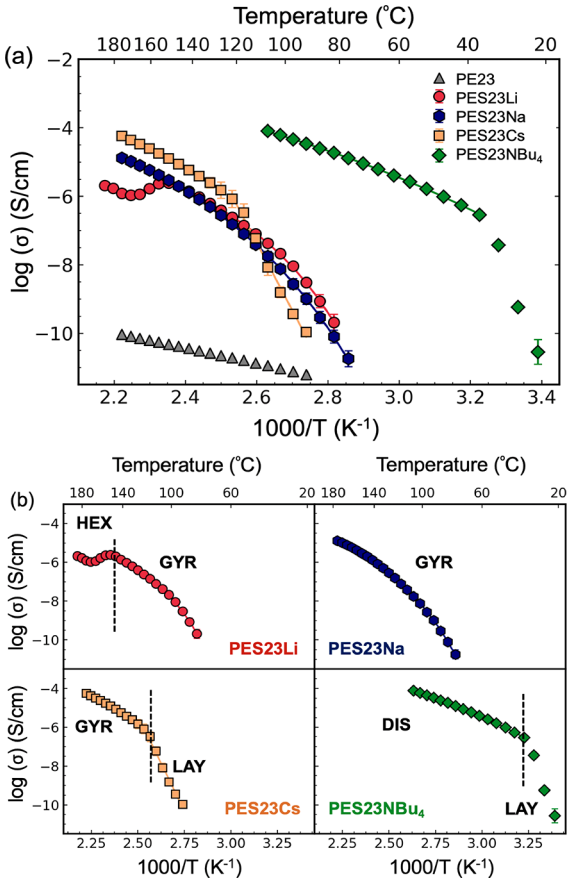

Figure 5. (a) Temperature-dependent ion conductivities of PES23 polymers during cooling at ~1 °C/min. (b) The ionic conductivities are presented separately to clarify the dependence on morphologies. Dashed lines indicate the phase boundary obtained from cooling in DSC. HEX, GYR, LAY, and DIS denote hexagonal, gyroid, layered, and disordered ionic aggregate morphologies, respectively.

PES23Na exhibit similar ionic conductivities between 80 and 160 °C. Increasing the counterion size from Li^+ or Na^+ to Cs^+ increases the ionic conductivity by nearly half an order of magnitude at temperatures above the T_m of PES23Cs. Exchanging the counterion to NBu_4^+ increases ionic conductivity by 2 orders of magnitude compared to the other PES23 polymers. The increase in ionic conductivity with increased counterion size is primarily attributed to weakened ion-pairing interactions, which not only lower the crystallization temperature by 70−90 °C but also enhance the mobility of ions by facilitating ion dissociation.[48] Note that NBu_4^+ cations are an informative comparison here to rationalize structure formation, but not of prime interest for energy applications. The ionic conductivities of all polymers at temperatures above the T_m are described well with a Vogel−Fulcher−Tammann (VFT) relationship,

$$\sigma = \sigma_\infty \exp\left(\frac{-D}{T - T_0}\right)$$

where D is inversely related to the fragility, and T_0 is the Vogel temperature, corresponding to an infinitely slow structural relaxation time. Fitting parameters are provided in Table S3. The VFT behavior at $T < T_m$ indicates that the ion transport in melt-state PES23 polymers is facilitated by the polymer segmental relaxation.[48,54,55]

Figure 5b shows the ion transport for each polymer separately to demonstrate the influence of morphology on the ionic conductivities. The ionic conductivity of PES23Li decreases on cooling from 190 °C until the onset of the hexagonal-to-gyroid OOT at 170 °C. The ionic conductivity increases by about a factor of 10 during this order-to-order phase transition until the transformation is completed at 150 °C. Then the σ continues to decrease with temperature in a VFT manner until the conductivity is too low to be measured. These results demonstrate that the formation of the interconnected gyroid ionic aggregate morphology is more efficient for ion conduction compared to the hexagonal shaped ionic aggregates in PES23Li. In contrast, the hexagonal to gyroid OOT for PES23Na at ~190 °C was not accessible in the conductivity measurement and the gyroid to layered OOT at ~125 °C is absent due to slow crystallization kinetics. Thus, the gyroid phase persists throughout the measured temperature window, and the ionic conductivities display a smooth VFT-like temperature dependence.

For PES23Cs and $PES23NBu_4$, the ion conduction displays a VFT behavior while the ionomers exhibit the gyroid or disordered ionic aggregates, respectively, in the melt state. As the temperature decreases to the onset of crystallization, the ionic conductivities show an abrupt decrease and exhibit Arrhenius-like temperature dependence,

$$\sigma = \sigma_0 \exp\left(\frac{-E_a}{RT}\right)$$

where σ_0 is the ionic conductivity at infinite high temperature, and E_a is the activation energy for ion transport. Such Arrhenius-like behavior suggests that ion transport in layered ionic aggregates embedded with crystalline PE backbone segments is decoupled from the polymer relaxations. A similar trend was also observed in our recent work on (i) low-molecular-weight monodisperse and telechelic polyethylenes forming semicrystalline ionic layered structures[46] and (ii) periodic polyethylene sulfonate ionomers with PE segments of 48 carbons.[49]

Ionic conductivities during the second heating from 25 °C were also investigated up to ~180 °C (Figure S11). Since PES23Na does not exhibit morphological change within the measured temperature window, the ionic conductivities are consistent between heating and cooling. For PES23Cs and $PES23NBu_4$, the ionic conductivities in the layered morphologies show a small discrepancy between first cooling and second heating due to differences in the crystal size and crystallinity during the cooling. Once the polymers become fully melted, the ionic conductivities are consistent between the cooling and heating cycles.

The phase transition hysteresis in PES23Li provides valuable insights regarding the morphological effects on ion transport. Figure 6 shows the ionic conductivities of PES23Li upon cooling (190 to 25 °C, ~1 °C/min) followed directly by a second heating (25 to 190 °C, ~1 °C/min). At high temperatures, we observed an increase in the ionic conductivity during cooling (solid symbols) when the hexagonal ionic aggregates transform into the gyroid ionic aggregates, while upon the second heating the ionic conductivity decreases during the gyroid-to-hexagonal OOT. In addition, during the gyroid-to-hexagonal OOT at 150−180 °C, the ionic conductivities during the second heating are higher than those measured in the first cooling and correspond

DOI: 10.1021/jacs.9b09701
J. Am. Chem. Soc. 2020, 142, 857−866

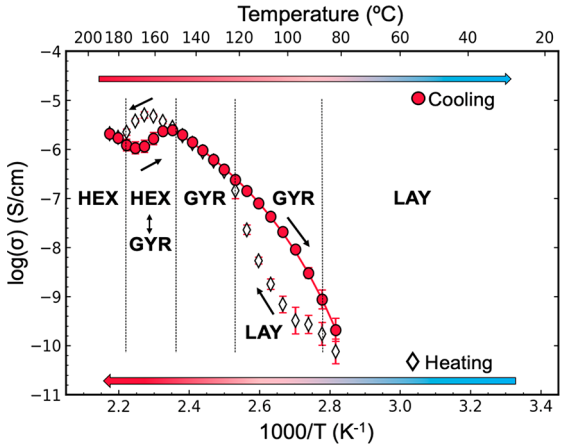

Figure 6. Ionic conductivity of PES23Li during the first cooling from 190 to 25 °C (solid) and second heating back to 190 °C (open). LAY, GYR, and HEX represent layered, gyroid, and hexagonal aggregate morphologies, respectively.

to the persistence of the gyroid phase. These results unequivocally demonstrate the higher ionic conductivity in the $Ia\bar{3}d$ cubical gyroid phase relative to the hexagonal phase in PES23Li.

To compare the ion transport in the gyroid and layered morphology, we measured the isothermal ionic conductivity of PES23Li after directly cooling from 190 to 100 °C (~1 °C/min). The slow crystallization of PES23Li, as mentioned in the thermal analysis section, allows the ionic conductivity to be probed as the amorphous gyroid structure evolves into the semicrystalline layered structure (Figure 7a). To capture the corresponding structural evolution, X-ray scattering data was also collected isothermally at 100 °C for a similar amount of time after cooling directly from 190 °C (~1 °C/min), Figure 7b–d.

Figure 7a shows that the ionic conductivity of PES23Li at 100 °C gradually decreases over ~8 h from ~5×10^{-8} to ~2×10^{-10} S/cm. X-ray scattering patterns at selected times during isothermal crystallization at 100 °C are shown in Figure 7b with the full patterns as a function over time shown as heatmaps in Figure 7c and 7d. After 20 min, X-ray data indicates that the ionic aggregates of PES23Li pack in a gyroid structure similar to the pattern in Figure 1. The appearance of a peak at lower q after 200 min suggests the coexistence of the gyroid structure and the layered structure. At 300 min, the layered structure dominates the overall ionic aggregate morphology and a crystalline peak at 1.48 $Å^{-1}$ appears. The transformation is completed after ~500 min, as evidenced from Figure 7c,d, which is consistent with a plateau in ionic conductivity. The ionic conductivity in the layered PES23Li is expected to depend on crystallinity, crystal domain sizes, grain boundary morphologies, etc., that will vary with crystallization conditions. Nonetheless, for this thermal treatment, we demonstrate that the bicontinuous gyroid phase is more efficient for ion conduction than the isotropic semicrystalline layered morphology in PES23Li. We attribute the more than 2 orders of magnitude higher ionic conductivity at 100 °C found for the gyroid morphology to the great connectivity of the ionic aggregates between grains. While challenges remain to make PES23 promising single ion conductor (i.e., dissociating the cations from the sulfonates), the ability of these polymers

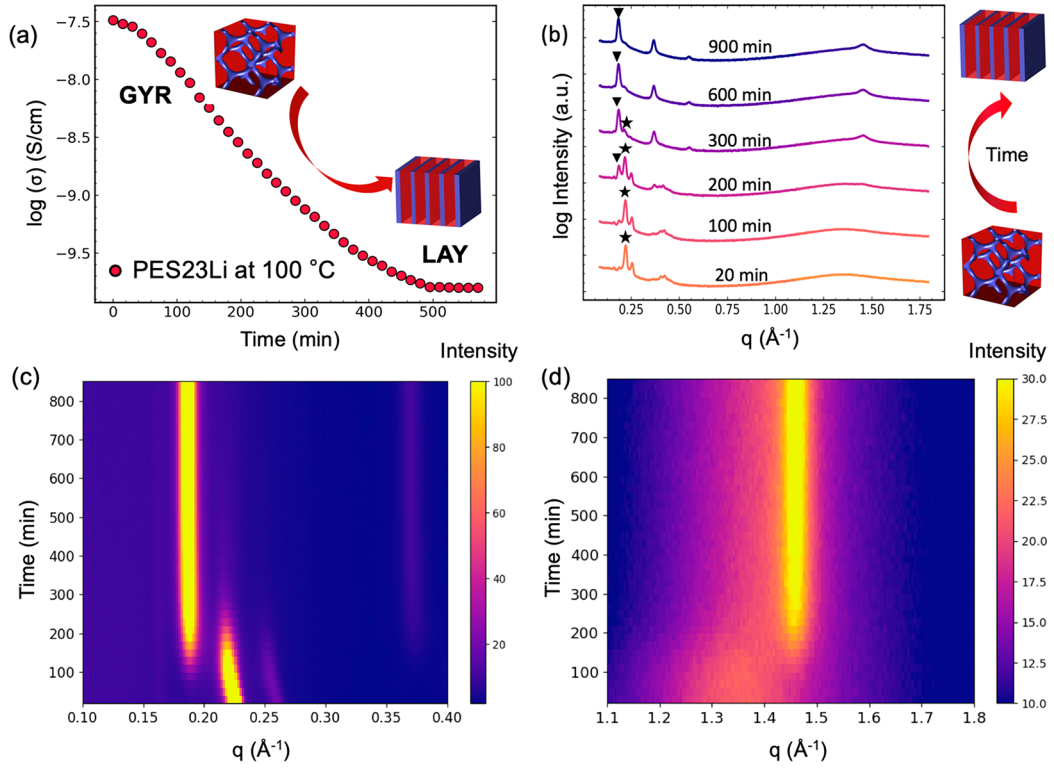

Figure 7. (a) Isothermal ionic conductivity of PES23Li as a function of time after cooling from 190 to 100 °C (~1 °C/min). (b) Time-dependent *in situ* X-ray scattering profiles of PES23Li after cooling from 190 to 100 °C. The stars and the triangles represent the first-order peak in the gyroid and layered morphologies, respectively. Isothermal (c) SAXS and (d) WAXS data of PES23Li after cooling from 190 °C to 100 °C as a function of time, where color indicates scattering intensity. Vertical strips correspond to peaks in I vs q data in (b).

DOI: 10.1021/jacs.9b09701
J. Am. Chem. Soc. 2020, 142, 857–866

to self-assemble into ordered gyroid ionic aggregates is an important step toward designing viable single-ion conductors.

CONCLUSION

Bicontinuous gyroid structures can be obtained for single-ion conducting polymers. This was established by studies of four periodic polyethylene sulfonates with different counterions, namely Li^+, Na^+, Cs^+, and NBu_4^+, and PE spacers of 23 carbon atoms. *In situ* X-ray scattering captured the morphological transitions as a function of temperature, including order-to-order transitions reminiscent of block copolymers. Driven by the crystallization tendency of the PE blocks, these polymers exhibit layered ionic aggregate morphologies with folded chain conformation near the polar blocks. The semicrystalline layered ionic aggregate morphologies transform directly into disordered ionic aggregates at $T < T_m$ for the ionomer with the largest cation, PES23NBu$_4$. More interestingly, PES23Li, PES23Na, and PES23Cs transition from layered ionic aggregates to bicontinuous gyroid ionic aggregates in an OOT at T_m. Furthermore, the gyroid morphologies in PES23Li and PES23Na transform into hexagonal ionic aggregates at a second OOT at higher temperatures. The order-to-order transitions in ionic aggregate morphologies were also evident in linear viscoelastic rheological measurements, which also highlight the potential for the bicontinuous gyroid structure to provide improved mechanical properties.

The symmetry of the ionic aggregate morphologies plays a critical role in ion transport. Particularly for PES23Li, we demonstrate that the bicontinuous gyroid morphology exhibits higher ion conductivities at a given temperature than the isotropic layered and hexagonal morphologies. These results demonstrate that the gyroid structure with its 3D interconnected ion-conducting pathways is a highly advantageous nanostructure for ion conduction in single-ion containing polymers. This study has established that the bicontinuous gyroid structure is available in single-ion conductors when the polymer backbone is amorphous, the polymer microstructures are well-defined, and the polar volume fraction is ∼0.28. The design rules established here should be broadly applicable as new single-ion conductors are envisioned.

ASSOCIATED CONTENT

Supporting Information

The Supporting Information is available free of charge at https://pubs.acs.org/doi/10.1021/jacs.9b09701.

Experimental methods; NMR spectra; DSC thermograms; in situ X-ray scattering profiles at all measured temperatures; representative crystallography information; ionic conductivities of PES23Na, PES23Cs, and PES23NBu$_4$ during cooling and heating (PDF)

AUTHOR INFORMATION

Corresponding Author

*winey@seas.upenn.edu

ORCID

Lu Yan: 0000-0002-5248-7821

Christina Rank: 0000-0003-1092-893X

Stefan Mecking: 0000-0002-6618-6659

Karen I. Winey: 0000-0001-5856-3410

Notes

The authors declare no competing financial interest.

ACKNOWLEDGMENTS

L.Y. and K.I.W. acknowledge funding by the National Science Foundation (DMR 1506726 and DMR 1904767). C.R. and S.M. acknowledge funding by the DFG (SFB1214). L.Y., K.I.W., and S.M. acknowledge support for travel by the Stiftung Baden-Württemberg (PRICON). We thank Chinedum Osuji and Ryan Poling-Skutvik for assistance with all the rheologic measurements. We also acknowledge the use of the Dual Source and Environmental X-ray Scattering facility operated by the Laboratory for Research on the Structure of Matter at the University of Pennsylvania (NSF MRSEC 17-20530). The equipment purchase was made possible by a NSF MRI grant (17-25969), an ARO DURIP grant (W911NF-17-1-0282), and The University of Pennsylvania. We thank Jinseok Park for helpful discussions.

REFERENCES

(1) Patel, S. N.; Balsara, N. P. Charge Transporting Nanostructured Polymers for Electrochemical Systems - a Themed Collection. *Mol. Syst. Des. Eng.* **2019**, *4*, 221−222.

(2) Morris, M. A.; An, H.; Lutkenhaus, J. L.; Epps, T. H. Harnessing the Power of Plastics: Nanostructured Polymer Systems in Lithium-Ion Batteries. *ACS Energy Lett.* **2017**, *2*, 1919−1936.

(3) Shi, Y.; Peng, L.; Ding, Y.; Zhao, Y.; Yu, G. Nanostructured Conductive Polymers for Advanced Energy Storage. *Chem. Soc. Rev.* **2015**, *44*, 6684−6696.

(4) Matyjaszewski, K.; Tsarevsky, N. Nanostructured Functional Materials Prepared by Atom Transfer Radical Polymerization. *Nat. Chem.* **2009**, *1*, 276−288.

(5) Morariu, M. D.; Voicu, N. E.; Schaffer, E.; Lin, Z.; Russell, T. P.; Steiner, U. Hierarchical Structure Formation and Pattern Replication Induced by an Electric Field. *Nat. Mater.* **2003**, *2*, 48−52.

(6) Cui, H.; Chen, Z.; Zhong, S.; Wooley, K. L.; Pochan, D. J. Block Copolymer Assembly via Kinetic Control. *Science* **2007**, *317*, 647−650.

(7) Bates, F. S.; Fredrickson, G. H. Block Copolymers-Designer Soft Materials. *Phys. Today* **1999**, *52*, 32−38.

(8) Bates, C. M.; Bates, F. S. 50th Anniversary Perspective: Block Polymers-Pure Potential. *Macromolecules* **2017**, *50*, 3−22.

(9) Bates, F. S.; Fredrickson, G. H. Block Copolymer Thermodynamics: Theory and Experiment. *Annu. Rev. Phys. Chem.* **1990**, *41*, 525−557.

(10) Lodge, T. P. Block Copolymers: Past Successes and Future Challenges. *Macromol. Chem. Phys.* **2003**, *204*, 265−273.

(11) Orilall, M. C.; Wiesner, U. Block Copolymer Based Composition and Morphology Control in Nanostructured Hybrid Materials for Energy Conversion and Storage: Solar Cells, Batteries, and Fuel Cells. *Chem. Soc. Rev.* **2011**, *40*, 520−535.

(12) Kato, T.; Yoshio, M.; Ichikawa, T.; Soberats, B.; Ohno, H.; Funahashi, M. Transport of Ions and Electrons in Nanostructured Liquid Crystals. *Nat. Rev. Mater.* **2017**, *2*, 17001.

(13) Robbins, S. W.; Beaucage, P. A.; Sai, H.; Tan, K. W.; Werner, J. G.; Sethna, J. P.; DiSalvo, F. J.; Gruner, S. M.; Van Dover, R. B.; Wiesner, U. Block Copolymer Self-Assembly−Directed Synthesis of Mesoporous Gyroidal Superconductors. *Sci. Adv.* **2016**, *2*, No. e1501119.

(14) Bates, F. S.; Hillmyer, M. a.; Lodge, T. P.; Bates, C. M.; Delaney, K. T.; Fredrickson, G. H. Multiblock Polymers: Panacea or Pandora's Box? *Science (Washington, DC, U. S.)* **2012**, *336*, 434−440.

(15) Elabd, Y. A.; Hickner, M. A. Block Copolymers for Fuel Cells. *Macromolecules* **2011**, *44*, 1−11.

(16) Hamersky, M. W.; Hillmyer, M. A.; Tirrell, M.; Bates, F. S.; Lodge, T. P.; Von Meerwall, E. D. Block Copolymer Self-Diffusion in the Gyroid and Cylinder Morphologies. *Macromolecules* **1998**, *31*, 5363−5370.

(17) Crossland, E. J. W.; Kamperman, M.; Nedelcu, M.; Ducati, C.; Wiesner, U.; Smilgies, D. M.; Toombes, G. E. S.; Hillmyer, M. A.;

DOI: 10.1021/jacs.9b09701
J. Am. Chem. Soc. 2020, 142, 857−866

Ludwigs, S.; Steiner, U.; Snaith, H. J. A Bicontinuous Double Gyroid Hybrid Solar Cell. *Nano Lett.* **2009**, *9*, 2807−2812.
(18) Ichikawa, T.; Yoshio, M.; Hamasaki, A.; Kagimoto, J.; Ohno, H.; Kato, T. 3D Interconnected Ionic Nano-Channels Formed in Polymer Films: Self-Organization and Polymerization of Thermotropic Bicontinuous Cubic Liquid Crystals. *J. Am. Chem. Soc.* **2011**, *133*, 2163−2169.
(19) Ichikawa, T.; Yoshio, M.; Hamasaki, A.; Taguchi, S.; Liu, F.; Zeng, X.; Ungar, G.; Ohno, H.; Kato, T. Induction of Thermotropic Bicontinuous Cubic Phases in Liquid-Crystalline Ammonium and Phosphonium Salts. *J. Am. Chem. Soc.* **2012**, *134*, 2634−2643.
(20) Soberats, B.; Yoshio, M.; Ichikawa, T.; Taguchi, S.; Ohno, H.; Kato, T. 3D Anhydrous Proton-Transporting Nanochannels Formed by Self-Assembly of Liquid Crystals Composed of a Sulfobetaine and a Sulfonic Acid. *J. Am. Chem. Soc.* **2013**, *135*, 15286−15289.
(21) Villaluenga, I.; Chen, C. X.; Devaux, D.; Hallinan, D. T.; Balsara, N. P. Nanoparticle-Driven Assembly of Highly Conducting Hybrid Block Copolymer Electrolytes. *Macromolecules* **2015**, *48*, 358−364.
(22) Jung, H. Y.; Mandal, P.; Jo, G.; Kim, O.; Kim, M.; Kwak, K.; Park, M. J. Modulating Ion Transport and Self-Assembly of Polymer Electrolytes via End-Group Chemistry. *Macromolecules* **2017**, *50*, 3224−3233.
(23) Ichikawa, T.; Kato, T.; Ohno, H. 3D Continuous Water Nanosheet as a Gyroid Minimal Surface Formed by Bicontinuous Cubic Liquid-Crystalline Zwitterions. *J. Am. Chem. Soc.* **2012**, *134*, 11354−11357.
(24) Roy, R.; Park, J. K.; Young, W. S.; Mastroianni, S. E.; Tureau, M. S.; Epps, T. H. Double-Gyroid Network Morphology in Tapered Diblock Copolymers. *Macromolecules* **2011**, *44*, 3910−3915.
(25) Shen, K.-H.; Brown, J. R.; Hall, L. M. Diffusion in Lamellae, Cylinders, and Double Gyroid Block Copolymer Nanostructures. *ACS Macro Lett.* **2018**, *7*, 1092−1098.
(26) Martínez-Veracoechea, F. J.; Escobedo, F. A. Lattice Monte Carlo Simulations of the Gyroid Phase in Monodisperse and Bidisperse Block Copolymer Systems. *Macromolecules* **2005**, *38*, 8522−8531.
(27) Roy, S.; Skoff, D.; Perroni, D. V.; Mondal, J.; Yethiraj, A.; Mahanthappa, M. K.; Zanni, M. T.; Skinner, J. L. Water Dynamics in Gyroid Phases of Self-Assembled Gemini Surfactants. *J. Am. Chem. Soc.* **2016**, *138*, 2472−2475.
(28) Zhai, C.; Zhou, H.; Gao, T.; Zhao, L.; Lin, S. Electrostatically Tuned Microdomain Morphology and Phase-Dependent Ion Transport Anisotropy in Single-Ion Conducting Block Copolyelectrolytes. *Macromolecules* **2018**, *51*, 4471−4483.
(29) Alshammasi, M. S.; Escobedo, F. A. Correlation between Ionic Mobility and Microstructure in Block Copolymers. A Coarse-Grained Modeling Study. *Macromolecules* **2018**, *51*, 9213−9221.
(30) Baez-Cotto, C. M.; Mahanthappa, M. K. Micellar Mimicry of Intermetallic C14 and C15 Laves Phases by Aqueous Lyotropic Self-Assembly. *ACS Nano* **2018**, *12*, 3226−3234.
(31) Cho, B. K.; Jain, A.; Gruner, S. M.; Wiesner, U. Mesophase Structure-Mechanical and Ionic Transport Correlations in Extended Amphiphilic Dendrons. *Science (Washington, DC, U. S.)* **2004**, *305*, 1598−1601.
(32) Kato, T.; Hamasaki, A.; Yoshio, M.; Ichikawa, T.; Ohno, H.; Mukai, T. Self-Organization of Room-Temperature Ionic Liquids Exhibiting Liquid-Crystalline Bicontinuous Cubic Phases: Formation of Nano-Ion Channel Networks. *J. Am. Chem. Soc.* **2007**, *129*, 10662−10663.
(33) Jo, G.; Ahn, H.; Park, M. J. Simple Route for Tuning the Morphology and Conductivity of Polymer Electrolytes: One End Functional Group Is Enough. *ACS Macro Lett.* **2013**, *2*, 990−995.
(34) Mogurampelly, S.; Borodin, O.; Ganesan, V. Computer Simulations of Ion Transport in Polymer Electrolyte Membranes. *Annu. Rev. Chem. Biomol. Eng.* **2016**, *7*, 349−371.
(35) Fragiadakis, D.; Dou, S.; Colby, R. H.; Runt, J. Molecular Mobility and Li(+) Conduction in Polyester Copolymer Ionomers Based on Poly(Ethylene Oxide). *J. Chem. Phys.* **2009**, *130*, 064907.
(36) Hallinan, D. T.; Balsara, N. P. Polymer Electrolytes. *Annu. Rev. Mater. Res.* **2013**, *43*, 503−525.
(37) Seitz, M. E.; Chan, C. D.; Opper, K. L.; Baughman, T. W.; Wagener, K. B.; Winey, K. I. Nanoscale Morphology in Precisely Sequenced Poly(Ethylene-Co-Acrylic Acid) Zinc Ionomers. *J. Am. Chem. Soc.* **2010**, *132*, 8165−8174.
(38) Buitrago, C. F.; Jenkins, J. E.; Opper, K. L.; Aitken, B. S.; Wagener, K. B.; Alam, T. M.; Winey, K. I. Room Temperature Morphologies of Precise Acid- and Ion-Containing Polyethylenes. *Macromolecules* **2013**, *46*, 9003−9012.
(39) Buitrago, C. F.; Opper, K. L.; Wagener, K. B.; Winey, K. I. Precise Acid Copolymer Exhibits a Face-Centered Cubic Structure. *ACS Macro Lett.* **2012**, *1*, 71−74.
(40) Buitrago, C. F.; Alam, T. M.; Opper, K. L.; Aitken, B. S.; Wagener, K. B.; Winey, K. I. Morphological Trends in Precise Acid- and Ion-Containing Polyethylenes at Elevated Temperature. *Macromolecules* **2013**, *46*, 8995−9002.
(41) Middleton, L. R.; Trigg, E. B.; Yan, L.; Winey, K. I. Deformation-Induced Morphology Evolution of Precise Polyethylene Ionomers. *Polymer* **2018**, *144*, 184−191.
(42) Trigg, E. B.; Middleton, L. R.; Yan, L.; Winey, K. I. Comparing Morphological Evolution during Tensile Deformation of Two Precise Polyethylenes via 2D Fitting of in Situ X-Ray Scattering. *Macromolecules* **2018**, *51*, 7942−7950.
(43) Trigg, E. B.; Stevens, M. J.; Winey, K. I. Chain Folding Produces a Multilayered Morphology in a Precise Polymer: Simulations and Experiments. *J. Am. Chem. Soc.* **2017**, *139*, 3747−3755.
(44) Yan, L.; Bustillo, K. C.; Panova, O.; Minor, A. M.; Winey, K. I. Solution-Grown Crystals of Precise Acid- and Ion-Containing Polyethylenes. *Polymer* **2018**, *135*, 111−119.
(45) Trigg, E. B.; Gaines, T. W.; Marechal, M.; Moed, D. E.; Rannou, P.; Wagener, K. B.; Stevens, M. J.; Winey, K. I. Self-Assembled Highly Ordered Acid Layers in Precisely Sulfonated Polyethylene Produce Efficient Proton Transport. *Nat. Mater.* **2018**, *17*, 725−731.
(46) Yan, L.; Häußler, M.; Bauer, J.; Mecking, S.; Winey, K. I. Monodisperse and Telechelic Polyethylenes Form Extended Chain Crystals with Ionic Layers. *Macromolecules* **2019**, *52*, 4949−4952.
(47) Wang, W.; Liu, W.; Tudryn, G. J.; Colby, R. H.; Winey, K. I. Multi-Length Scale Morphology of Poly(Ethylene Oxide)-Based Sulfonate Ionomers with Alkali Cations at Room Temperature. *Macromolecules* **2010**, *43*, 4223−4229.
(48) Tudryn, G. J.; Liu, W.; Wang, S.-W.; Colby, R. H. Counterion Dynamics in Polyester-Sulfonate Ionomers with Ionic Liquid Counterions. *Macromolecules* **2011**, *44*, 3572−3582.
(49) Rank, C.; Yan, L.; Mecking, S.; Winey, K. I. Periodic Polyethylene Sulfonates from Polyesterification: Bulk and Nanoparticles Morphologies and Ionic Conductivities. *Macromolecules* **2019**, *52*, 8466−8475.
(50) Thomas, E. L.; Sass, S. L. On the Orthorhombic to Hexagonal Phase Transformation in Polyethylene Single Crystals. *Makromol. Chem.* **1973**, *164*, 333−341.
(51) Tashiro, K.; Sasaki, S.; Kobayashi, M. Structural Investigation of Orthorhombic-to-Hexagonal Phase Transition in Polyethylene Crystal: The Experimental Confirmation of the Conformationally Disordered Structure by X-Ray Diffraction and Infrared/Raman Spectroscopic Measurements. *Macromolecules* **1996**, *29*, 7460−7469.
(52) Hall, L. M.; Stevens, M. J.; Frischknecht, A. L. Effect of Polymer Architecture and Ionic Aggregation on the Scattering Peak in Model Ionomers. *Phys. Rev. Lett.* **2011**, *106*, 127801.
(53) Sing, C. E.; Zwanikken, J. W.; Olvera De La Cruz, M. Electrostatic Control of Block Copolymer Morphology. *Nat. Mater.* **2014**, *13*, 694−698.
(54) Wang, S.-W.; Colby, R. H. Linear Viscoelasticity and Cation Conduction in Polyurethane Sulfonate Ionomers with Ions in the Soft Segment−Multiple Phase Systems. *Macromolecules* **2018**, *51*, 2767−2775.

DOI: 10.1021/jacs.9b09701
J. Am. Chem. Soc. 2020, 142, 857−866

(55) Klein, R. J.; Zhang, S.; Dou, S.; Jones, B. H.; Colby, R. H.; Runt, J. Modeling Electrode Polarization in Dielectric Spectroscopy: Ion Mobility and Mobile Ion Concentration of Single-Ion Polymer Electrolytes. *J. Chem. Phys.* **2006**, *124*, 144903.

DOI: 10.1021/jacs.9b09701
J. Am. Chem. Soc. 2020, 142, 857−866